Available online at www.elixirpublishers.com (Elixir International Journal)

Nanotechnology

Elixir Nanotechnology 96 (2016) 41689-41695

ISSN: 2229-712X

Effect of Lithium doping on Structural, Optical, Eletrochemical and Magnetic Properties of NiO Nanoparticles

R. Shanaj Begum and R. John Xavier*

Department of Physics, Periyar EVR College (Autonomous), Tiruchirappalli – 620 023, India.

ARTICLE INFO

Article history:

Received: 16 June 2016;

Received in revised form: 15 July 2016;

Accepted: 21 July 2016;

Keywords

Lithium doping,
Electro chemical activity,
Specific capacitance,
Ferromagnetism.

ABSTRACT

Pure Nickel Oxide (NiO) nanoparticles and Lithium doped Nickel Oxide nanoparticles at two different concentrations 0.01M, 0.02M were synthesized through co-precipitation method. From XRD analysis it is observed that all the three samples exhibit FCC cubic structure and the incorporation of lithium decreases the crystallite size with increase in the Li doping concentration. Optical absorption spectra reveal that the energy gap increases from 3.8 eV to 3.98 eV with increasing lithium doping concentration. The Photoluminescence spectra show that the PL intensity increases with increase in lithium content. The SEM images clearly show an agglomeration of nanoparticles and snowflake-like morphology. Cyclic voltammetry characterization was carried out for all the three samples to study electrochemical activity. The magnetic property of the samples was studied using a vibrating sample magnetometer (VSM).

1.Introduction

Nickel Oxide (NiO) is a P-type transition metal oxide semiconductor that has rock salt (NaCl) structure and a wide energy band gap in the range 3.6 eV to 4.0 eV. It is an anti ferromagnetic [1], electro chromic [2], catalytic [3] chemically stable [4], high transparency and electrical conductivity [5] and gas sensing material [6]. Due to electrochromism property, it is widely used in smart windows, electrochemical super-capacitors and dye-sensitized photo cathodes.

The Optical, Electrical and Magnetic properties of metal Oxide nanoparticles mainly depend on the size of the nanoparticles. The addition of impurity atoms known as doping [7-9] enhances these properties. More recently lithium doped NiO nanoparticles are widely used due to their less resistivity, high electro chemical reactivity and sensor response. Due to their unique properties, Lithium doped NiO NPs are utilized in gas sensing units, Pollutant clean-up catalysts, alkaline battery cathodes, dye sensitized solar cells and lithium ion batteries [10-13].

Several methods are used to synthesis Pure NiO and lithium doped NiO nanoparticles like hydrothermal [14], thermal decomposition [15], sol-gel [16], combustion [17], mechanosynthesis [18], pyrolysis [19]. Surfactant-mediated method [20], simple liquid phase process [21] and other techniques [22, 23].

In this article, well crystalline pure NiO and lithium doped NiO nanoparticles with different concentration were synthesized by a simple process called co-precipitation method [24] which is effective and low cost since the starting materials are few and inexpensive.

2. Material and methods

2.1 Synthesis

Nickel oxide nanoparticles and Lithium doped Nickel oxide nanoparticles have been synthesized through co-precipitation method. An aqueous solution containing a mixture of Nickel (II) Chloride (Aldrich ,98%) and Lithium chloride (Aldrich, 99%) in an appropriate amount of $Ni_{0.2-x}Li_xO$ (x=0, 0.01 and 0.02M) is used to synthesis pure and Lithium doped nickel oxide nanoparticles.

$NiCl_2$ and $LiCl_2$ at different concentrations (x=0 M, 0.01M and 0.02M) were dissolved in 100 ml of de-ionized water and were stirred for 2 hours.100 ml of Sodium hydroxide (1.6 M) solution was added to the solution drop wise under constant stirring. The resultant solution was stirred for 6 hours and was refluxed at room temperature for 24 hours. The green precipitate obtained was washed with double distilled water and ethanol to remove impurity. The sample was dried by heating at 90°C in air and then calcined for 5 hrs at 700°C, the greenish sample turned into black color powder. The above procedure was repeated for x= 0.01M and 0.02M to synthesis Li doped NiO nanoparticles.

2.2 Characterization.

The samples were analyzed by Powder X-Ray Diffraction (XRD) using X' Pert PRO Diffractometer with Cu K_α radiation of wave length 0.15406 nm in 2θ range of 10°- 80° operated at 40 kV and 30 mA. Fourier Transform Infrared (FT-IR) spectroscopy analysis, UV-Vis spectroscopy analysis, (Instrument model Lamda 35) and Photoluminescence spectroscopy analysis (model-LS45) were used to analyze optical property of the samples. Morphology of NiO NPs was studied by Scanning electron microscopy (SEM). Cyclic Voltammetry experiment was performed using three electrode cell utilizing computer controlled potentiostat (Princeton, Applied Research-Versa STAT MC–AMETEK). Vibrating sample magnetometer was used to study the magnetic property of the samples.

2.3 Electrochemical Characterization

Cyclic voltammetry analysis was done using a three electrode electrochemical cell consisting of a glassy carbon electrode, saturated calomel electrode (SCE), platinum electrode as the working electrode, the reference electrode and counter electrode respectively.

Tele: +91 94430 73908
E-mail address: rj_xavier@yahoo.com

The Nickel Oxide NPs were added to water which acts as solvent. Ethyl Tri methyl Ammonium Bromide which acts as electrolyte was added to the test solution to ensure sufficient conductivity. The potential is swept between-1.4 V and 1.8V at a scan rate of 20 mVs^{-1}. The current flowing through working electrode is recorded as a function of the varying potential. The same procedure was repeated for Li doped nickel oxide nanoparticles.

3. Results and discussions

3.1 Structural Analysis

Fig.1 shows XRD patterns of pure NiO nanoparticles (S1) and lithium doped NiO nanoparticles (S2 and S3) at different lithium concentrations. In all the samples diffraction peaks are indexed as (111), (200), (220), (311) and (222) crystal planes which correspond to cubic structure (pure NiO-JCPDS: 78-0429, Li doped NiO-JCPDS : 89-3605, Fm-3m space group) without any impurity peak. From fig.1, it is evident that Lithium doped samples do not show peaks related to metallic lithium which confirm that the cubic phase of NiO remains unaffected by the incorporation of lithium ions. As the lithium dopant increases, intensity of the peaks decreases and FWHM of the peak increases which leads to decrease in crystallite size.

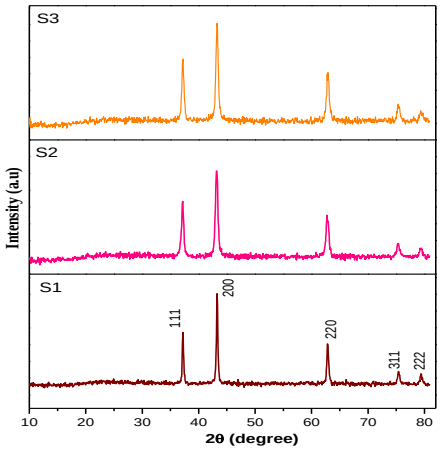

Fig 1. XRD spectra of (S1) NiO, (S2) Li: NiO (x=0.01M) and (S3) Li: NiO (x=0.02M).

The size of the crystallite was estimated by Debye-Scherer formula [25] as follows

$$D = K\lambda/\beta \cos(\theta) \quad (1)$$

Where k=0.9, D is the crystallite size, λ is the wavelength of the Cu-Kα radiation (1.5406 A°), β is the full width at half maximum intensity and θ is the peak position. The average crystallite size of the samples S1, S2 and S3 is 39 nm, 27 nm and 25 nm respectively. As the lithium content increases the crystallite size decreases which are due to the fact that doping process inhibits the nucleation and the subsequent growth rate of nickel oxide nanoparticles [26].

Assuming that the particle size and strain contributions to peak broadening are independent of each other and both have Cauchy like profile, the observed line breadth is sum of the two i.e. $\beta = (k\lambda/D\ \cos\theta) + (4\varepsilon\sin\theta)$ which becomes

$$\beta\cos\theta = (k\lambda/D) + 4\varepsilon\sin\theta \quad (2)$$

By using the above Williamson-Hall formula [27], a graph was plotted with 4sinθ along the X-axis and βcosθ along the Y-axis. From the linear fit, Strain (ε) and the size of the crystallite are calculated from the slope and y-intercept of the fitted line respectively (Fig. 2). The crystallite size estimated from Scherer formula is found to be small due to peak broadening caused by micro strain and dislocations compared to the crystallite size obtained by W.H analysis. (Table 1)

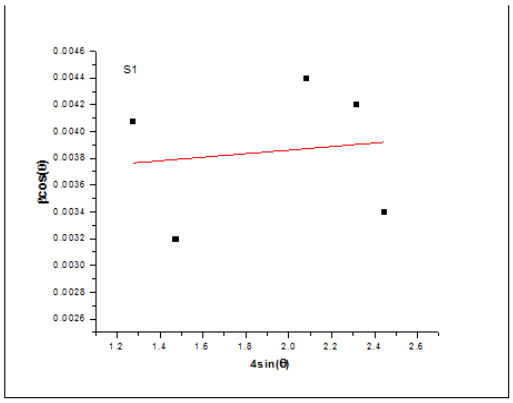

Fig 2a.

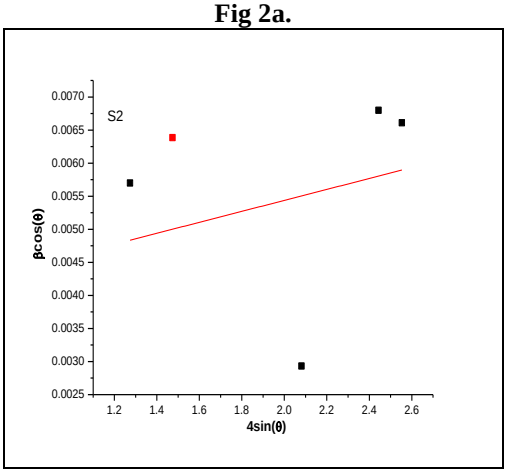

Fig 2b.

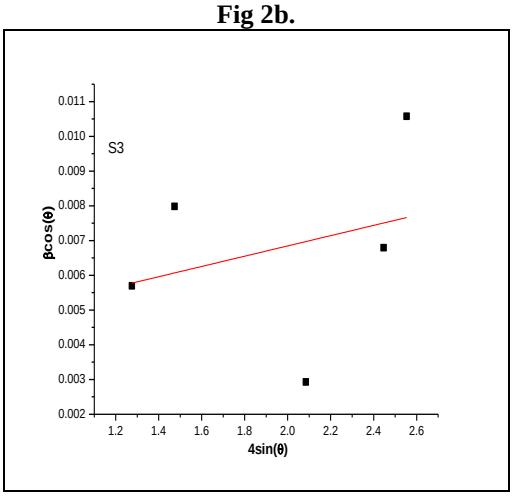

Fig 2c.

Figs 2. W-H Plot for (S1) NiO, (S2) Li: NiO (x=0.01M) and (S3) Li: NiO (x=0.02M).

The micro strain (ε) induced in the samples due to imperfection and distortions and the dislocation density (δ) which represents amounts of defects [28] are estimated using the expression (3) and (4) and the values are listed in Table 1

$$\varepsilon = \frac{\beta}{4\tan\theta} \quad (3)$$

$$\delta = 1/D^2 \quad (4)$$

Where β is the full width at half maximum intensity and θ is the peak position, D is the grain size in nm. It is apparent from Table 1 that the crystallite size decreases with the increasing

dopant concentration but the dislocation density and the micro strain are increasing.

Table 1.XRD parameter values for undoped NiO and Lithium doped NiO nanoparticles.

Samples	crystallite size (nm)		Microstrain $*10^{-3}$	Dislocation density (δ) ($*10^{14}$) Lines/m^2
	Scherer's formula	W-H plot		
S1	39	40	2.43	6.11
S2	27	37	3.12	17.86
S3	25	35	3.64	27.34

The inter planer spacing between the atoms (d) is calculated using Bragg's law.

$2d\sin\theta = n\lambda$ (5)

The lattice constant 'a' can be determined using the expression

$a = d*(h^2+k^2+l^2)^{½}$ (6)

The particle size, value of 'd' and the lattice constant 'a' determined for the samples S1, S2 and S3 at maximum peak intensity (200) are listed in Table 2.

Table 2. Size and d-spacing of undoped NiO and Lithium doped NiO nano particles atMaximum peak intensity (200).

Samples	Position 2θ (^{0})	FWHM (β) (^{0})	Crystallite size (nm)	Calculated d-value(A°)	Lattice parameter (A°)
S1	43.2653	0.1968	43	2.0895	4.1820
S2	42.2410	0.3936	22	2.0906	4.1846
S3	43.2290	0.4920	17	2.0912	4.1858

It is apparent that as the Lithium content increases ,the peaks show small shift towards lower values of 2θ which increases both the inter planer spacing between the atoms (d) and the lattice parameter [29] and also the substitution of Li^+ ions (r_{ion} = 0.76A°) in the Ni^{2+} (r_{ion} = 0.69A°) vacancies in normal crystal position results in increased lattice constant.

3.2 Fourier Transform Infrared (FT-IR) Spectroscopic Analysis

Fig. 3 shows the FT-IR spectra of the pure NiO NPs (S1) and doped NiO samples (S2, S3). The absorption bands at 3412 cm^{-1}, 3419 cm^{-1} and 3404 cm^{-1} for the samples S1, S2 and S3 respectively are the characteristic of O–H stretching bond.

The weak absorption peaks are observed at 1597 cm^{-1} for S1, 1630 cm^{-1} for S2 and 1663 cm^{-1} for S3 are attributed to H-O-H bending vibration because of absorption of water molecule from air as the sample is synthesized in air. The bands due to carbonate groups are observed at 1393 cm^{-1} and 1119 cm^{-1} for S1, 1449 cm^{-1}, 1368 cm^{-1}, 1044 cm^{-1} for S2 and 1442 cm^{-1}, 1371cm^{-1}, 1044 cm^{-1} for S3. The band at 722 cm^{-1} for pure NiO NPs and 690 cm^{-1} for lithium doped NiO NPs are assigned to Ni–O–H vibration mode [30].

It is clear from the spectra (Figs. 3b and 3c) of S2 and S3 that when the lithium content is increased, the same functional groups are appeared with a slight change in the intensity and frequency of the bands. The absorption bands below 1000 cm^{-1} confirm metal-oxygen i.e Li-O and Ni-O vibration [31]. These absorption bands arise due to inter atomic vibrations [32]. It is important to note that strong bands exist at 492 cm^{-1} pure NiO NPs [33] and 429 cm^{-1}, 419 cm^{-1} for the lithium doped samples S2 and S3 confirm the formation of Ni-O [34,35]. Hence it is apparent that there is no change in the crystal structure of Nickel Oxide nanoparticles when lithium is doped which is also confirmed by XRD analysis.

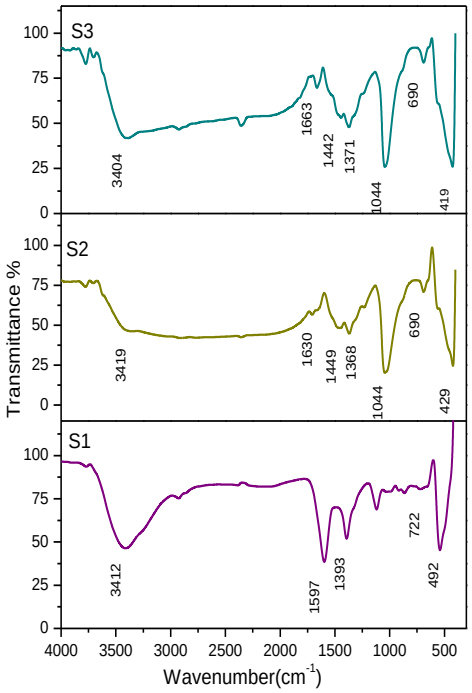

Fig 3. FT-IR spectra of NiO (S1), Li:NiO samples (S2) and (S3) for (x=0.01M,0.02M).

3.3 UV analysis

Fig. 4 shows Tauc's plots of pure NiO NPs (S1) and Lithium doped NiO NPs (S2, S3) and the insets show corresponding UV-Vis absorption spectra. The peak absorption intensity appears at 325 nm for NiO and at 224 nm and 221nm for Li doped samples S2 and S3 respectively. The incorporation of Lithium into NiO, shifts the peak absorption wavelengths towards lower number and further decreases with the increase of Lithium content. This effect is due to the generation of new discrete energy levels by chemical defects or vacancies present in the intergranular region [36]. Since NiO is a semiconductor with direct electronic transitions [37], the optical energy band gap (E_g) is calculated using Tauc's model [38]

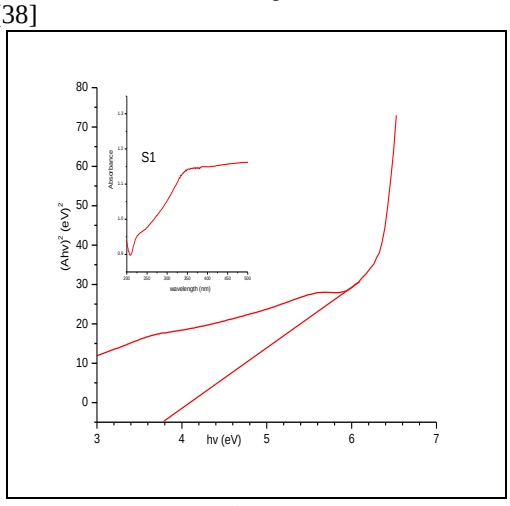

Fig 4a.

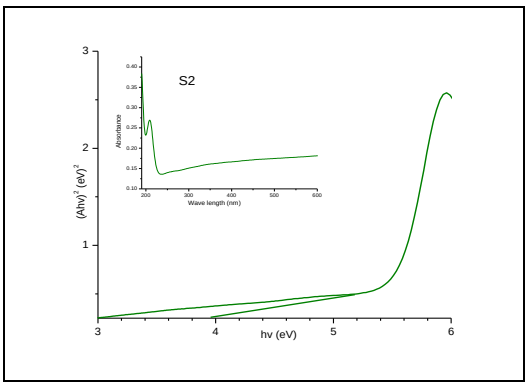

Fig 4b.

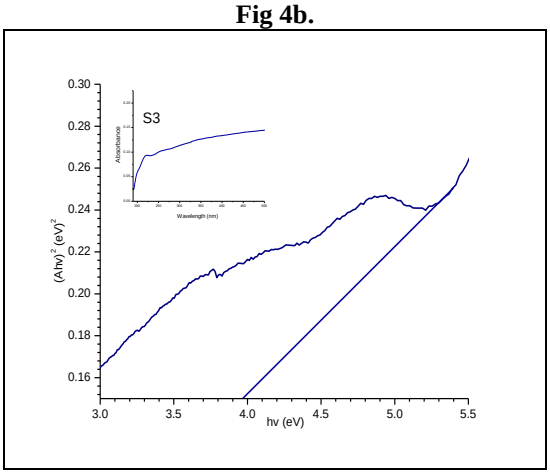

Fig 4c.

Figs 4. Tauc's plot for (S1) NiO, (S2) Li: NiO (x=0.01M) and (S3) Li: NiO (x=0.02M) and insets show absorption spectra.

$$(Ah\nu)^n = k\,(h\nu - E_g) \quad (7)$$

Where A is the absorbance constant, $h\nu$ is the photon energy and n = 2 for direct band gap. The graph of $(Ah\nu)^2$ as a function of $h\nu$ is plotted and the extrapolation of the linear portion of the curve to energy axis determines optical energy gap of the samples (Table 3). The obtained band gap values of undoped NiO NPs and lithium doped doped NiO NPs are less than that of band gap value of bulk NiO which is 4.0 eV [39,40]. It is found that the band gap energy increases from 3.8 eV (NiO) to 3.98 eV (Li-NiO) [41] due to decrease in crystallite size which is an evidence of the quantum confinement effect.

Table 3. Optical Parameters of undoped NiO and Lithium doped NiO nanoparticles.

Samples	Lithium Concentration (M)	Energy gap (eV)	Transmittance %
S1	0	3.80	13
S2	0.01	3.95	73
S3	0.02	3.98	91

3.4 Photoluminescence Analysis

The room temperature Photoluminescence spectra of Nickel Oxide nanoparticles and lithium doped Nickel Oxide nanoparticles are shown Fig. 5. The sample S1 excited by 290 nm exhibits main emission peak at 364 nm.The doped samples S2, S3 excited by 294 nm exhibit the main peaks at 326 nm, 320 nm in the UV region. The change in the emission peaks confirms the substitution of Li^+ ions in Ni^{2+} lattice sites. The optical absorption study reveals that there are several transitions at energies below the band gap energy of Nickel Oxide**.**The broad peaks in PL spectra of the samples are due to radiative recombination between electrons in the conduction band and holes in the valence band. As it is evident from Table 4. the emission peaks are shifted to higher PL energy as the particle size decreases from 39 nm to 27nm and 25 nm with increasing lithium concentration. This is due to the fact that oxygen vacancy is more in smaller size particles which makes absorption more hence it causes stronger PL signal. Hence the size of crystallite and doping concentration are the main factors in the variation of PL intensity. It is concluded that the PL intensity increases with increase in lithium content. The sample S1 exhibit weak visible emission at 479 nm due to defects-related deep level emissions like oxygen vacancies and Ni interstitials [43 ,44].But the lithium doped NiO nanoparticles did not show any deep level emissions which corresponds to indirect band gap where electrons from conduction band recombine with the holes in the valance band indirectly through traps without the emission of photons.

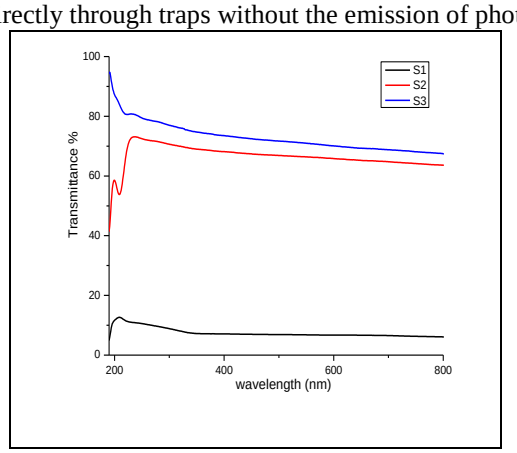

Fig 5. Transmittance spectra of the samples S1, S2 and S3.

3.5 Electrochemical Analysis

Fig. 6 compares the cyclic voltammograms of the undoped Nickel Oxide sample S1 and Lithium doped Nickel Oxide samples (S2 and S3) in the potential range of -1.3 V to 1.3V, at a sweep rate of 20 mVs^{-1}. It is apparent that there is a pair of strong redox peaks appear in all the three samples which indicate that capacitance characteristics are controlled by Faradic reactions [45]. The redox peaks occur according to equation (8) in pure nickel oxide nanoparticles due to Ni^{2+} to Ni^{3+} transition at the surface of NiO nanoparticles [46].

$$NiO + OH^- \longleftrightarrow NiOOH + e^- \quad (8)$$

The formation of NiOOH layer on the surface initiates the electro catalytic activity of NiO NPs. [47, 48].

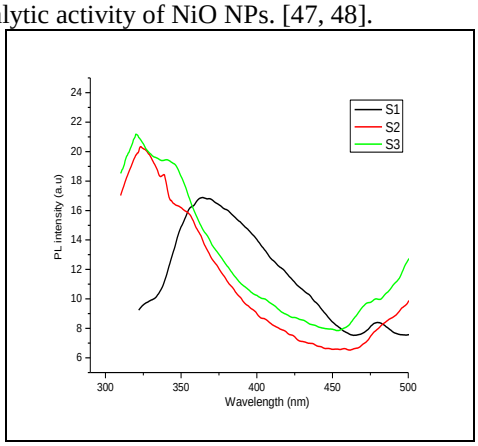

Fig 6. Photoluminescence intensity comparison of undoped NiO (S1) and Lithium doped NiO samples (S2 and S3).

In lithium doped nickel oxide nanoparticles the electrochemical activity is accompanied by the uptake and

release of electrons and lithium ions to maintain electrical neutrality within Li_yNiO. Acceding to equations (9) and (10), the insertion of Li^+ ions into NiO takes place by initial activation followed by a reversible reaction between Li_yNiO and $Li_{(y-z)}NiO$ [49-52].

$$NiO + y\,Li^+ + ye^- \longrightarrow Li_yNiO \quad (9)$$

$$Li_yNiO \longleftrightarrow Li_{(y-z)}NiO + z\,Li^+ + z\,e^- \quad (10)$$

The experimental results reveal that peak current (I_{pa}) of undoped Nickel Oxide NPs is higher than lithium doped Nickel Oxide NPs (S2 and S3). And also as the Li dopant concentration increases the peak current further decreases. It is due to the fact that when Lithium is doped in NiO, Li may not be readily ionized and some may act as neutral impurities in the NiO matrix. Specific capacitance is calculated by the formula,

$$C = \int_{E1}^{E2} i(E)\,dE / (2\,(E_2 - E_1)\,m\,v) \quad (11)$$

Where $\int_{E1}^{E2} i(E)\,dE$ is the total voltammetric charges obtained by integration of positive and negative sweep in cyclic voltammogram . Since the anodic voltammetric charges and cathodic voltammetric charges are not same in the CV curves ***integral area of CV curve/Scan rate*** represent the sum of anodic and cathodic voltammetric charges [53,54].

$(E_2 - E_1)$ is the potential window width, 'm' mass of the sample and v is the scan rate.

The electrochemical measurements show that samples S1, S2 and S3 exhibit specific capacitance of 834 Fg^{-1}, 832 Fg^{-1} and 800 Fg^{-1} respectively. Obviously undoped NiO nanoparticles exhibit the maximum specific capacitance compared to Li doped NiO nanoparticles. It is apparent that there is a decline of specific capacitance with the increased concentration of lithium.

The position of the peaks on the potential axis (E_p) is related to the formal potential of the redox process. The formal potential for a reversible couple is centered between anodic peak potential (E_{pa}) and cathodic peak potential (E_{pc}) [55]

$$E^0 = (E_{pa} + E_{pc})/2 \quad (12)$$

The separation between the peak potentials ΔE_p is evaluated using the relation

$$\Delta E_p = E_{pa} - E_{pc} = 59mV/n \quad (13)$$

Where n is the number of electrons. The ΔE_p for the samples S1, S2 and S3 is 0.843, 0.829V, and 0.939 V respectively. Thus, the peak separation can be used to determine the number of electrons transferred, and as a criterion for a Nernstian behavior. A fast one-electron transfer would exhibit a ΔEp = 0.059 V at 298 K **[**56**]**. The discrepancy from this ideal value is attributed to slow electron transfers and solution resistance.

3.6 Morphological analysis

SEM images of the undoped NiO sample S1, Li doped NiO samples S2 and S3 at different magnifications are shown in Fig. 7. The SEM images of undoped NiO (S1) clearly show an agglomeration of the nanoparticles and snowflakes like morphology. The incorporation of Li ions into NiO crystal lattice (S2 and S3) lead to variation in the morphology and a slight decrement in agglomeration and dispersion of crystallites with increasing lithium concentration.

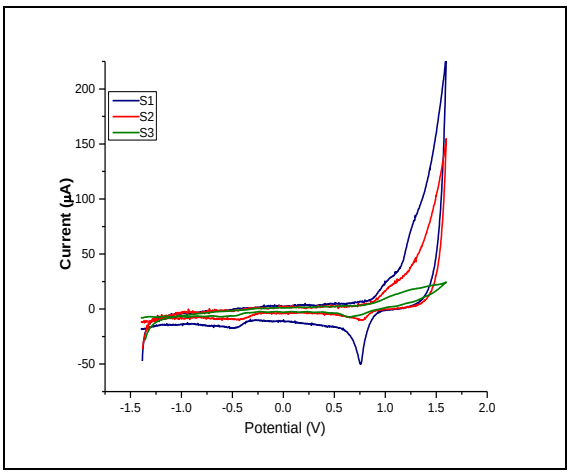

Fig7. Cyclic voltammograms for (S1)undoped NiO, (S2) Li:NiO (x=0.01M) and (S3)Li:NiO (x=0.02M).

3.7 Magnetic Properties

Fig. 8 shows Hysteresis loops for undoped NiO nanoparticles(S1) and Lithium doped NiO nanoparticles (S2 and S3) at room temperature with the maximum applied field of 2 ± 0.02 Tesla. Ferromagnetic behavior is observed in all the three samples although NiO bulk material is antiferromagnetic [57]. The saturation magnetization (M_s), coercivity (Hc) and retentivity(H_r) of all the samples are listed in Table 4. The saturation magnetization (M_s), retentivity (H_r) of the samples is increased with decreasing crystallite size on Li doping. It is due to the fact that the generation of holes on Li doping in NiO causes double exchange coupling through Li induced holes [58] and also net magnetic moment created in Li:NiO samples is greater than undoped NiO sample due to its reduced crystallite size which leads to large surface to volume ratio and increased lattice parameter.

Table 4.PL Energy of undoped NiO and Lithium doped NiO nanoparticles.

Samples	Emission Peaks (nm)	PL Intensity (a.u)	PL Energy (eV)
S1	364	16.90	3.408
S2	326	20.33	3.803
S3	320	21.17	3.875

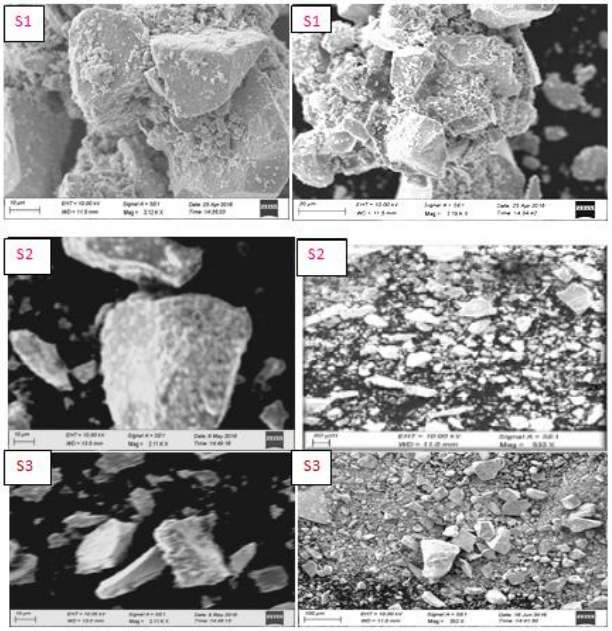

Fig 8. SEM images of (S1) un doped NiO, (S2) Li:NiO (0.01M) and (S3) Li:NiO (0.02M).

Table 5. Magnetic parameters of undoped NiO and Li doped NiO nanoparticles.

Samples	Lithium Concentration (M)	Ms (emu/g) *10^{-3}	Mr (emu/g *10^{-3}	Hc Tesla
S1	0.00	5.74	0.50	0.0802
S2	0.01	12.73	0.83	0.0699
S3	0.02	16.40	1.28	0.0390

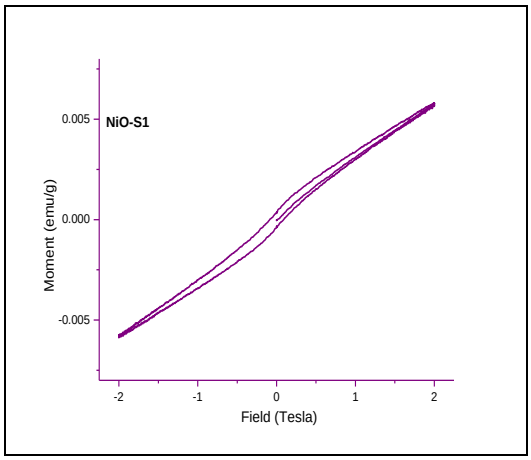

Fig. 9a

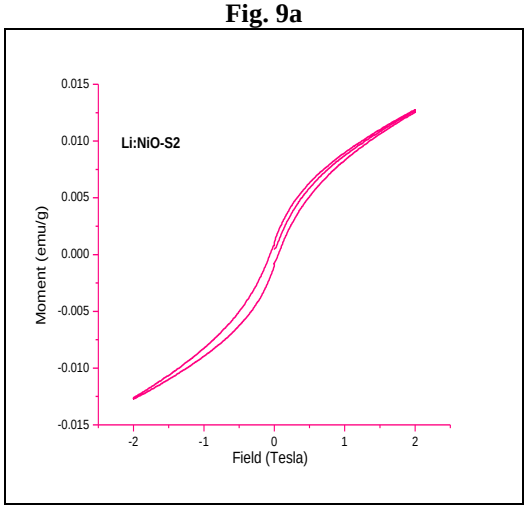

Fig. 9b

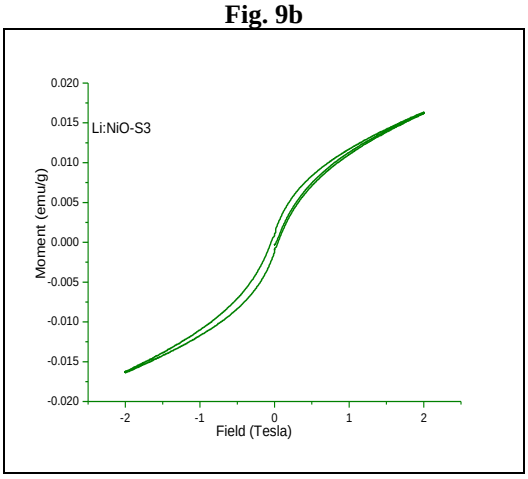

Fig 9c.

Figs 9. Hysteresis loops for (S1) undoped NiO, (S2) Li:NiO (x=0.01M) and (S3) Li:NiO (x=0.02M).

4. Conclusion

XRD analysis has revealed that doping of Li^+ ion into NiO and increase in Li^+ content decreases the crystallite size of the nickel oxide nanoparticles and increases lattice parameter which leads to expansion of unit cell. SEM analysis shows that the lithium doping produces change in shape of the samples as compared with NiO nanoparticles. It is evident from electrochemical characterization that specific capacitance of the samples decreases as lithium doping concentration increases. The increase in saturation magnetization and retentivity of the samples with the increase of Lithium concentration is due to reduction in crystallite size. The increase in optical band gap with the Li concentration reveals that Li:NiO nanoparticles are suitable material for Li:NiO based optoelectronic devices.

References

1. Sato A , Minami T, Takata S, Yamada T (1993), Thin solid films, 23, 27-31.
2. Bouessay I, Rougier A, Beaudoin B ,Leriche J.B (2002), Applied Surface Science, 186- 490.
3. Turky A.M (2003), Applied Catalysis A: General, 247-83.
4. Kumagai H, Matsumoto M, Toyoda K, Obara M (1996). J. Materials Science Letters, 15-1081.
5. Jlassi M, Sta I, Hajji M, Ezzaouia H (2014), Materials Science in Semiconductor Processing, 21-7.
6. Hotovy V.R.I , Siciliano P, Capone S, Spiess L (2002), Sensing characteristics of NiO thin films as NO2 gas sensor, Thin Solid Films, 418, 9.
7. Hsu L.S, Yeh C.S, Kuo C.C, Huang B.R , Dhar S (2005), J. Optoelectron. Adv. Mater, 7, 3039–3046.
8. Bhargava R.N, Haranath D , Metha A, Korean (2008) J. Phys.Soc, 53, 2847–2851.
9. Bae S.Y, Na C.W, Kang J. H , Park J (2005). J. Phys. Chem. B, 109, 2526–2531.
10. Vidotti M, Salvador R.P, Córdoba de Torresi S.I.(2009), Synthesis and characterization of stable Co and Cd doped nickel hydroxide nanoparticles for electrochemical applications, Ultrasonics Sonochemistry, 16, 35–40.
11. Sonavane A.C, Inamdar A.I, Shinde P.S, Deshmukh H.P, Patil R.S ,Patil P.S,(2010), Efficient electrochromic nickel oxide thin films by electro deposition. J. Alloys and Compounds, 489, 667–673.
12. Salavati-Niasari M, Mir N , Davar F (2010). A novel precursor in preparation and characterization of nickel oxide nanoparticles via thermal decomposition approach. J. Alloys and Compounds, 493, 163–168.
13. Wu M.S, Wang M.J , Jow J.J (2010). Fabrication of porous nickel oxide film with open macropores by electrophoresis and electro deposition for electrochemical capacitors. J.Power Sources, 195, 3950–3955.
14. Hirano S.L (1987), Am. Ceram. Soc. Bull-66, 1342–1344.
15. Xiang L, Deng X.Y, Jin Y (2002), Experimental study on synthesis of NiO nano-particles, Scripta. Mater. 47, 219–224.
16. Vorkapic D, Matsoukas T (1998), J. Am. Chem. Soc, 81,2 815–2820.
17. Williams D K, Bihari B, Tissue B M, McHale J M (1998). Preparation and fluorescence spectroscopy of bulk monoclinic Eu^{3+}:Y_2O_3 and comparison to Eu^{3+}:Y_2O_3 nanocrystals. J. Phys. Chem. B, 102, 916-920.
18. Gaffet E ,Tillement O (1997). Mechanochemistry and mechanical activation. Ann. Chim. 22, 417-422.
19. Ledoux G, Leconte Y, Amans D, Dujardin C, Combemale L (2007). Host Size Effects on Optical Properties of Y2O3:Eu3+ and Gd2O3:Eu3+ Nanoparticles Synthesized by Laser Pyrolysis.In Doped Nanopowders:Synthesis, Characterization Applications ; Trans Tech Publications LTD, 128, 157-163.

20. Wang Y.D, Ma C.L, Li H.D (2002), Inorg. Chem. Commun, 5, 751.
21. Wang C.B, Gau G.Y, Gau S.J, Tang C.W, Bi J.L (2005). Catal. Lett.101, 241.
22. Tao D, Wei F (2004). Mater. Lett. 58, 3226.
23. Wang Y, Ke J.J (1996). Mater. Res. Bull. 31, 55 .
24. Chauhan R, Kumar A, Chaudhary R.P (2010). J. Chem. Pharm. Res. 2, 178–183.
25. Cullity B.D, Stock S.R (2001), Elements of X-Ray Diffraction, (third ed.), Prentice Hall, Upper Saddle River, New Jersey.
26. Wang Y, Zhang L, Li .S, Jena P (2009). Polyol-mediated synthesis of ultrafine TiO2 nanocrystals and tailored physiochemical properties by Ni doping. J. Physical Chemistry C, vol.113, no. 21, pp. 9210–9217.
27. Wiley J.B and Kaner R.B (1992), J. Science 255, 1093.
28. Brigin V, Kose S ,Atay S ,Akyus I, The effect of substrate temperature on the structural and some physical properties ultrasonically sprayed CdS films.Materials chemistry and physics .Vol .93, pp.103.
29. Jang W.L , Lu Y.M, Hwang W.S, Chen W.C.(2010). Electrical properties of Li-doped NiO films. Eur. Ceram. Soc. 30, 503.
30. Sharanabasava V.Ganachari, Ravishankar Bhat,Raghunandan Deshpande , Venkataraman A (2012).Synthesis and characterization of nickel oxide nanoparticles by self-propagating, ISSN:2076-5061.
31. Tarascon J. M, Mckinnon W. R, Coowar F, Bowmer T. N, Amatucci G, Guyomard D (1994). Synthesis condition and oxygen. J.Electrochem. *Soc*. 141: 1421-1427.
32. Sun L, Li H, Ren L ,Hu C (2009). Synthesis of Co3O4 nanostructures using a solvothermal approach. Solid State Sciences, 11**,** 108-112.
33. Kanthimathi M , Dhathathreyan A ,Nair B.V (2004).Nanosized nickel oxide using bovine serum albumin as template, Mater. Lett. 58, 2914–2917.
34. Mayya K.M, Jain N, Gole A, Langevin D, Sastry M (2004). J.Colloid and Interface Science 270, 133–139.
35. Gnanachari S.V, Bhat R , Deshpande R , Venkataraman A (2012). Synthesis and characterization of nickel oxide nanoparticles by self-propagating low temperature combustion method. Recent Research in Science and Technology, 4**,** **5**0-53.
36. Song X, Gao L (2008). Facile Synthesis of Polycrystalline NiO Nanorods Assisted by Microwave Heating, J. Am. Ceram. Soc. 91, 3465–3468.
37. Li X, Zhang X, Li Z, Qian Y (2006).Synthesis and characteristics of NiO nanoparticles by thermal decomposition of nickel dimethyl glyoximate rods, Solid State Commun. 137, 581–584.
38. Tauc J (1966), The optical constants are determined by three methods; one of them is new and Properties of Solids, Academic Press, Inc**.** New York**.**
39. Jarzebski Z.M (1973) Oxide Semiconductors, Pergamon Press, Oxford. 150, 184.
40. Adler D, Feinleib J (1970). Phys. Rev. B. 2, 3112.
41. Kamal H, Elmaghraby E K, Ali S.A, Abdel-Hady K (2004). Characterization of nickel oxide films deposited at different substrate temperatures using spraypyrolysis, J. Cryst. Growth 26, 424.
42. Joseph D P, Saravanan M, Muthuraaman B, Renugambal P, Sambasivam S (2008).Spray deposition and characterization of nanostructured Li- doped NiO thin films for application in dye-sensitized solar cells. Nanotechnology; 19, 485707.
43. Zhou M.H ,Yu J.G, Liu S.W, Zhai P.C and Jiang L. (2008).Effects of calcination temperatures on photocatalytic activity of SnO2/TiO2 composite films prepared by an EPD method. J. Hazardous Materials, 154, 1–3, 1141–1148.
44. Manna S, Deb A.K, Jagannath J, De S.K (2008). Synthesis and room temperature ferromagnetism in Fe doped NiO nanorods. J. Phys. Chem. C, 112, 10659.
45. Dubal. D. P. Jagadale A. D , Patil. S. V, Lokhande C. D (2012) Materials Research Bulletin 47, 1239.
46. Mao-Sung Wu , Min-Jyle Wang (2010).Nickel oxide film with open macropores fabricated by surfactant-assisted anodic deposition for high capacitance supercapacitors.J. Chem. Commun., vol. 46, pp. 6968–6970.
47. Tong X, Qin Y, Guo X, Moutanabbir O, Ao X. (2012).Enhanced catalytic activity for methanol electro-oxidation of uniformly dispersed nickel oxide nanoparticles - carbon nanotube hybrid materials. 8(22), 3390–3395.
48. Rahim A, Abdel Hameed R, Khalil M (2004). Nickel as a catalyst for the electro-oxidation of methanol in alkaline medium. J. Power Sources 134(2), 160–169.
49. Passerini S, Scrosati B, Gorenstein A. (1990). The intercalation of lithium in nickel oxide and its electrochromic properties, J. Electrochem. Soc.137, 3297-3300.
50. Passerini S, Scarminio J, Scrosati B, Zane D, Decker F (1993). Thin metal oxide films on transparent substrates for Li-insertion devices, J. Appl. Electrochem. 23, 1187-1195.
51. Decker F, Passerini S, Pileggi R, Scrosati B (1993). The electro chromic process in non-stoichiometric nickel oxide thin film electrodes, Electrochim. Acta 37, 1033-1038.
52. Passerini S, Scrosati B (1992), Electrochromism of thin-film nickel oxide electrodes, Solid State Ionics53–56, 520-524.
53. Li H, Wang J, Chu Q, Wang Z, Zhang F , Wang S (2009). J. Power Sources 2009, 190, 578.
54. Nam K.W, Lee C.W, Yang X.Q, Cho B.W, Yoon W.S, (2009), J. Power Sources,188, 323.
55. Bard A. J, Faulkner L. R., (2001)..Electrochemical Methods: Fundamentals and Applications, John Wiley & Sons, Hoboken, NJ, USA.
56. Eisele S, Schwarz M, Speiser B, Tittel C, [2006]. Electrochim. Acta; 51: 5304.
57. Ngo P, Bonville P, Pileni M.P (1999). Nanoparticles of CoxFeyzO4: synthesis and super paramagnetic properties, Eur. Phys. J B 9583–592.
58. Lin Y H, Zhan B, Nan C W, Zhao R, Xu X, Kobayashi M (2011). Ferro magnetism in antiferromagnetic NiO-based thin films. J. Appl. Phys.110, 043921-4.